Exergetic, economic, and environmental evaluations and multi-objective optimization of a combined molten carbonate fuel cell-gas turbine system

Alireza Haghighat Mamaghani [a], Behzad Najafi [b], Ali Shirazi [c, *], Fabio Rinaldi [b]

[a] *Scuola di Ingegneria Industriale, Campus di Piacenza, Politecnico di Milano, Via Scalabrini, 76, 29100, Piacenza, Italy*
[b] *Dipartimento di Energia, Politecnico di Milano, Via Lambruschini 4, 20156, Milano, Italy*
[c] *School of Mechanical and Manufacturing Engineering, The University of New South Wales (UNSW), Kensington, New South Wales, 2052, Australia*

Received 15 May 2014
Accepted 5 December 2014
Available online 13 December 2014

1. Introduction

Fuel cell systems are an appropriate alternative to conventional power generation systems specifically in micro scale distributed systems due to their relatively high efficiency and lower environmental effects [1–4]. Molten carbonate fuel cells (MCFCs) are high-temperature fuel cells in which a molten carbonate salt mixture is employed as the electrolyte [5]. In order to allow an effective ion conduction and avoid rapid voltage degradation, their operating temperature should be between 600 °C and 700 °C, which is high enough to provide fast kinetics and eliminate the need for a noble metal catalysts [6]. The high operating temperature and pressure of the MCFCs also makes them highly suitable to use in combined heat and power applications (CHP) [7]. Moreover, the high operating temperature enables MCFCs to internally reform fuels such as natural gas or landfill gas [8]. One alternative approach for enhancing the efficiency of MCFC systems is to integrate fuel cells with other power generators such as gas turbines [9–12], turbo expanders [13], or micro-gas turbines [14]. Accordingly, molten carbonate fuel cell (MCFC)/gas turbine (GT) hybrid system has attracted a great attention due to its higher efficiency [15].

Some of the previous works have been specifically focused on the mathematical modeling of the MCFC [16] and MCFC stack with internal reforming [17], while many research activities were dedicated to the analysis of the hybrid MCFC systems. Leto et al. [11] modeled a hybrid system consisting of a MCFC coupled with a micro-turbine, and also performed a sensitivity analysis by varying main operating parameters. They demonstrated that this system could reach electrical and overall efficiencies up to 60% and 70% respectively. El-Emam and Dincer [18] conducted energetic and exergetic analyses of an MCFC-GT system and obtained overall energetic and exergetic efficiencies of 42.9% and 37.75%, respectively. In addition, Rashidi et al. [13] conducted a similar study on an MCFC-Gas turbine system and achieved an overall energetic efficiency of 57.4%, exergetic efficiency of 56.2%, bottoming cycle energetic efficiency of 24.7% and stack energetic efficiency of 43.4%. In another study, an MCFC operated at ambient pressure and

* Corresponding author. Tel.: +61 413077896.
E-*mail addresses:* alireza.haghighat@mail.polimi.it (A.H. Mamaghani), behzad.najafi@mail.polimi.it (B. Najafi), a.shirazi@student.unsw.edu.au (A. Shirazi), fabio.rinaldi@polimi.it (F. Rinaldi).

Nomenclature

A	area (m^2)
c_f	fuel unit cost (USD MJ^{-1})
CRF	capital recovery factor
$\dot{C}_{env}$	social cost of air pollution (USD s^{-1})
$\dot{C}_{tot}$	total cost rate (USD s^{-1})
C_{cold}	heat capacity rate of cold flow
C_{hot}	heat capacity rate of hot flow
E	open circuit voltage (V)
e	specific exergy (kJ kg^{-1})
$\dot{E}$	exergy flow rate (kW)
$\overline{e}$	specific exergy (kJ $kmol^{-1}$)
F	Faraday constant (96,485C mol^{-1})
h	specific enthalpy (kJ kg^{-1})
$\overline{h}$	specific enthalpy (kJ $kmol^{-1}$)
I	current (A)
J	current density (A m^{-2})
i	interest rate (%)
K	equilibrium constant
LHV	low heating value (kJ kg^{-1})
$\dot{m}$	mass flow rate (kg s^{-1})
N	operational hours in a year
n	system lifetime (year)
$\dot{n}$	molar flow rate (kmol s^{-1})
P	pressure (bar)
$\dot{Q}$	the time rate of heat transfer, kW
R	resistance (Ω m^{-2})
$\overline{R}$	universal gas constant (kJ kmol K^{-1})
r	pressure ratio
s	specific entropy (kJ kg^{-1} K^{-1})
$\overline{s}$	specific entropy (kJ $kmol^{-1}$ K^{-1})
S/C	steam to carbon ratio
T	temperature (K)
TIT	turbine inlet temperature (K)
U_f	fuel utilization factor
V	voltage (V)
$\dot{W}$	mechanical work (kW)
x	molar fraction
Z	capital cost USD
$\dot{Z}$	capital cost rate (USD s^{-1})

Greek symbols

ε	effectiveness
η	efficiency
Φ	maintenance factor
Ψ	exergetic efficiency

Subscripts

an	anode
B	burner
cat	cathode
C	compressor
CC	combustion chamber
Ch	chemical
D	destruction
El	electrochemical
f	fuel
G	electric generator
Gen	generated
HE-1	heat exchanger
HRE	heat recovery exchanger
ir	irreversibility
M	mixer
ne	nernst
Ph	physical
R	reformer
RHE	recovery heat exchanger
tot	total
T	turbine
WGS	water gas shift

combined with a STIG cycle was examined and efficiencies up to 69% were obtained [19]. In another research, it was observed that an MCFC with 46.4% efficiency has the capability of being integrated with a steam generation power system in order to achieve an overall efficiency of nearly 70% [20]. Akkaya and Sahin [21] investigated the energetic performance of a combined system consisting of an SOFC and an ORC running with R-113. The results revealed that the efficiency of the SOFC-ORC system is 14–25% higher than the efficiency of single SOFC because of the waste heat recovery through ORC.

In order to perform a comprehensive assessment of a power generation unit, economic aspects of the system should also be taken into account. Monaco and Di Matteo [22] performed an economic analysis of a 2.5 kW MCFC unit employing the life cycle assessment. Hengeveld and Revankar [3] carried out an economic analysis on a combined heat and power molten carbonate fuel cell system. They demonstrated that, in the case of extremely high electrical energy cost and low natural gas cost, this system becomes economically reasonable, leading to a satisfying payback period of 10 years. Dicks and Siddle [23] investigated the commercial prospects of MCFCs in different countries and markets. They proposed that a range of 300–400 kW might be the best choice for initial market entry. Moreover, thermo-economic optimization of a MCFC hybrid system has been conducted by Verda and Nicolin [9]. In their study, the design which results in an efficiency of 0.46, leads to the minimum cost of electricity of 0.036 USD per kWh. Sciacovelli and Verda [10] performed multi objective optimization of a MCFC-Gas turbine plant and investigated the effect of considering uncertainties such as methane conversion in the steam reformer, landfill gas composition and ambient temperature on the achieved set of optimal solutions.

In the recent years, due to the increasing environmental concerns, the amount of emission produced by power generation plants has been considered as a crucial issue. A method for investigating the environmental impact of MCFC in its lifetime has been proposed by Monaco and Di Matteo [22]. Shirazi et al. [24] conducted thermal-economic-environmental analysis and multi-objective optimization of a solid oxide fuel cell-gas turbine hybrid system. CO, NO_x and CO_2 emission costs were taken into account in the total cost rate of the cycle and minimized in the optimization process.

Although many work has been carried out on the modeling and optimization of MCFC based hybrid plants, no through study on the optimization of such systems, considering thermal, economic and environmental viewpoints, has been performed. Motivated by this research gap, in the present study, a comprehensive thermodynamic model of a hybrid MCFC-GT plant is first developed, which evaluates the behavior of the system from energetic and exergetic standpoints. An economic model is developed in order to estimate the total cost of the system including the capital cost, operating

cost, and the social cost due to the emissions of the system. Finally, the multi-objective optimization of the system is performed to achieve the optimal design point of the system.

2. Mathematical modeling

2.1. System description

The schematic diagram of the hybrid MCFC system is shown in Fig. 1. The plant is fed by natural gas. Air (stream 7) is pressurized via the air compressor (C), and then is mixed with the burner (B) high temperature outlet steam (stream 19) and the resulting mixture (stream 13) is directed to the cathodic side of the MCFC stack. Likewise, the natural gas (stream 5) is first mixed with steam (stream 4) produced in a heat exchanger (HE-1), and then this flow is preheated (stream 10) in the recovery heat exchanger (RHE) with the reformer outlet stream (stream 11). Stream 10 enters the reformer (R), where methane is converted into hydrogen, carbon monoxide, carbon dioxide and water. The required heat for reforming reactions is supplied by the burner. The hydrogen-rich stream (stream 11) is cooled down in the RHE to reach the desired temperature, and then enters the anode side of MCFC stack to participate in the electrochemical reaction. The electrochemical reaction in the MCFC stack also generates thermal energy which is partly utilized to heat up the cell products and residual reactants. The cathodic side outlet (stream 15) is split into two streams. The first stream (stream 16) is mixed with the anodic side outlet (stream 14), and then is directed to the burner where the remaining methane, carbon monoxide and hydrogen is completely burned with excess air to produce necessary heat for reformer. The second one (stream 18) is directed to the combustion chamber (CC) where the residual carbon monoxide is burnt with appropriate amount of fuel. The resulting flue gas (stream 9) which has a high temperature passes through the gas turbine (*T*) where it expands and provides the required power for the air compressor. Furthermore, additional useful work produced via flue gas expansion in the turbine is converted to electrical power using a generator (G). The high temperature stream leaves the turbine (stream 1), is fed to the heat exchanger to heat up the liquid water (flow 3). The high temperature flue gas (stream 2) leaving the HE-1 provides the choice to utilize the remaining thermal energy in this stream for co-generation purposes. To achieve this goal, a heat exchanger (HRE) is employed to heat up water for further uses, and the exhaust gas is finally discharged to the atmosphere (stream 23). The fuel cell and gas turbine electrical power outputs strongly depend on the operating parameters; however the nominal values can be estimated to be around 100 kW and 40 kW for stack and gas turbine electrical power output respectively.

2.2. Energy analysis

A thermodynamic model of the plant, based on the energetic analysis, is presented in this section. The following assumptions have been taken into account while developing the model of the system:

- Cathode and anode temperatures are supposed to be the same at the outlets.
- Steady state operation is considered for all components, which implies there is neither accumulation of energy nor mass in the whole system through the time. Moreover, regarding the electrode kinetics, steady state means the electrode pores have no mass accumulation capacities and products of the reactions transfer into and out of the electrodes at the same time reactions happen.
- Natural gas is assumed to be pure methane.
- There is no heat loss from the reformer, fuel cell stack, and the burner to the surroundings.
- Heat exchangers, mixer, compressor and the turbine are adiabatic; hence, there is no heat transfer between these systems and the surrounding environment.
- Electrolyte migration is not considered.

2.2.1. Compressor

The required power of the air compressor is provided by the turbine. The isentropic efficiency of the compressor (η_C) is defined as follows:

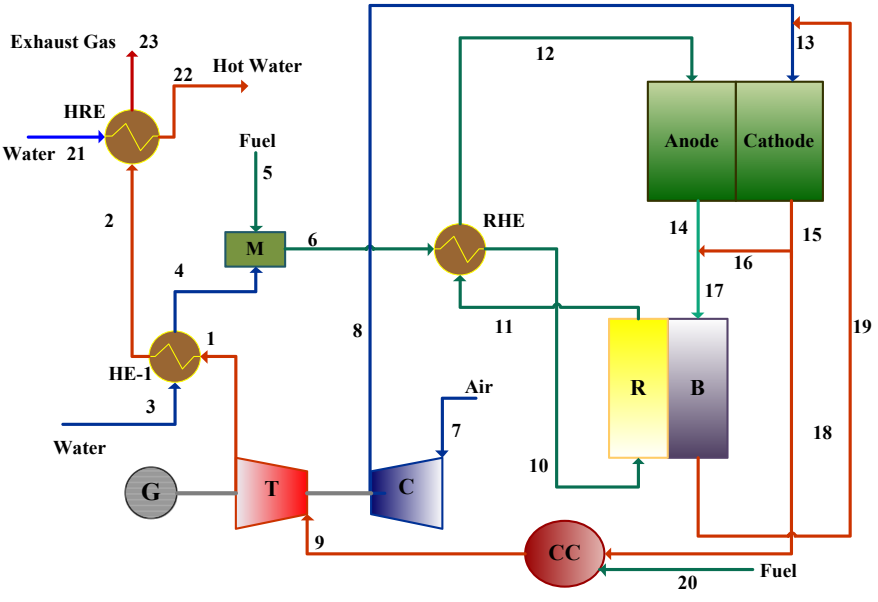

Fig. 1. Schematic diagram of MCFC-GT hybrid plant with heat recovery system.

$$\eta_C = \frac{h_{8,S} - h_7}{h_8 - h_7} \quad (1)$$

Applying the energy balance on the compressor, the compressor required power is:

$$\dot{W}_C = \dot{m}_8 h_8 - \dot{m}_7 h_7 \quad (2)$$

2.2.2. Burner

In order to calculate the flue gas temperature exiting the burner, the following energy balance for the burner is considered:

$$\dot{m}_{17} h_{17} - \dot{m}_{19} h_{19} = \dot{Q}_B \quad (3)$$

where $\dot{Q}_B$ is the heat produced by burner which is transferred through the heat exchange walls to the reformer.

2.2.3. Turbine

As illustrated in Fig. 1, gas turbine provides the required power of the air compressor while the remaining produced power will be the net mechanical power output.

$$\dot{W}_T = \dot{m}_9 h_9 - \dot{m}_1 h_1 \quad (4)$$

In this equation $\dot{W}_T$ is the net mechanical power output from the turbine.

2.2.4. Heat exchangers

The heat exchangers are modeled using the ε-NTU method in which the effectiveness can be found using effective heat transfer coefficient and surface area.

The effectiveness of the heat exchanger is defined as:

$$\varepsilon = \frac{C_{cold}(T_{cold,out} - T_{cold,in})}{C_{\min}(T_{hot,in} - T_{cold,in})} \quad (5)$$

C_{cold} is the heat capacity rate of the cold flow and the $C_{\min}$ is the minimum between C_{cold} and C_{hot} which is the heat capacity rate of the hot flow.

In addition, considering the fact that there is no heat loss from heat exchangers, the energy balance can be considered as:

$$\dot{m}_{hot,in} h_{hot,in} + \dot{m}_{cold,in} h_{cold,in} = \dot{m}_{hot,out} h_{hot,out} + \dot{m}_{cold,out} h_{cold,out} \quad (6)$$

2.2.5. Combustion chamber

A portion of the cathodic outlet stream (stream 18) and sufficient amount of fuel enter the combustion chamber and the fuel is burnt to provide a specific temperature for turbine inlet stream. Assuming a 2% of the total transferred heat as the heat loss from chamber to the environment, the gas temperature leaves the burner can be determined by the following energy balance for the CC:

$$\dot{m}_{18} h_{18} + \dot{m}_{20} h_{20} = \dot{m}_9 h_9 + \dot{Q}_{loss} \quad (7)$$

2.2.6. Reformer

Steam reforming reactions take place in the reformer to produce the required hydrogen for electrochemical reaction in the anode. Reactions occurring in the reformer are mainly endothermic (except the water gas shift reaction) and the required energy $\dot{Q}_B$ is provided by the hot flue gas from the burner. The following reactions are considered to take place in the reactor:

$$CH_4 + H_2O \Leftrightarrow CO + 3H_2$$

$$CH_4 + CO_2 \Leftrightarrow 2CO + 2H_2$$

$$CO + H_2O \Leftrightarrow CO_2 + H_2$$

The kinetic parameters for the reaction rates are extracted from Ref. [25]. The correlations given in the same reference were also employed for conducting heat transfer calculations within the reformer.

2.2.7. MCFC stack

The anodic side inlet flow is composed of hydrogen, water, unconsumed methane, carbon monoxide and carbon dioxide. The hydrogen generated in the reformer reacts with carbonate ions (CO_3^{2-}) which have passed through the membrane and produce water, carbon dioxide and electrons. These electrons are transferred to the cathode through an external circuit. Beside the electrochemical reaction, water gas shift reaction in the presence of CO also occurs in the anodic side.

The equilibrium constant of the water gas shift reaction can be calculated using the following relation [26]:

$$K_{WGS} = e^{\frac{4276}{T} - 3.961} \quad (8)$$

where T is the temperature of the stack. The equilibrium constant of shifting reaction can also be expressed in terms of partial pressures [26]:

$$K_{WGS} = \frac{P_{CO_2} P_{H_2}}{P_{CO} P_{H_2O}} \quad (9)$$

Assuming that y and x are the molar flow rates of H_2 and CO participating in the electrochemical and water gas shift reactions respectively:

$$K_{WGS} = \frac{(\dot{n}_{CO_2,12} + x + y).(\dot{n}_{H_2,12} + x - y)}{(\dot{n}_{CO,12} - x).(\dot{n}_{H_2O,12} - x + y)} \quad (10)$$

$$y = U_f(\dot{n}_{H_2,12} + x) \quad (11)$$

$$U_f = \frac{\dot{n}_{H_2,12} - \dot{n}_{H_2,14}}{\dot{n}_{H_2,12}} \quad (12)$$

Knowing the stack temperature, the equilibrium constant can be calculated from Eq. (8), and x and y are determined by solving Eqs. (10)–(12) simultaneously.

2.2.7.1. Current, current density, cell potential and irreversibilities. The MCFC fuel cell current (I) can be determined based on the molar flow rate of hydrogen (y) consumed during the electrochemical reaction in the fuel cell as follows:

$$I = 2Fy \quad (13)$$

where F is the Faraday constant.

The fuel cell operating voltage can be calculated using the following relation:

$$V = E - \eta_{ne} - jR_{tot} \quad (14)$$

where E is the maximum theoretically achievable reversible potential, η_{ne} is the Nernst loss, j is the current density, and R_{tot} is the sum of irreversibilities occurring at the anode, the cathode and the electrode.

$$E = \frac{-\Delta G}{2F} \tag{15}$$

where ΔG is the change in molar Gibbs free energy of formation at standard pressure, The Gibbs free energy change may be expressed as function of temperature:

$$\Delta G = -242000 + 45.8T \tag{16}$$

where T is the stack temperature (K).

$$\eta_{ne} = \frac{\overline{R}T}{2F} \times \ln \frac{P_{CO_2,cat} \cdot P_{H_2,an} \cdot P_{O_2,cat}^{0.5}}{P_{H_2O,an} \cdot P_{CO_2,an}} \tag{17}$$

$$y = U_f\left(\dot{n}_{H_2,12} + x\right) \tag{18}$$

where P is the species average partial pressure in cell, and 'an' and 'cat' denote anodic and cathodic sides, respectively.

As a result of several types of irreversible losses in a real cell, the actual operating voltage of MCFC is less than the reversible one. The total irreversible losses, R_{tot}, consist of over potentials and cell resistance:

$$R_{tot} = R_{an} + R_{cat} + R_{ir} \tag{19}$$

where R_{an} and R_{cat} are irreversible losses of anode and cathode, respectively, and R_{ir} is the internal cell resistance. Losses for MCFCs may be calculated by the following equations [26]:

$$R_{an} = C_a \cdot e^{\frac{\Delta H}{RT}} \cdot P_{H_2,an}^{-0.5} \tag{20}$$

$$R_{cat} = C_1 \cdot e^{\frac{\Delta H_{C1}}{RT}} \cdot P_{O_2,cat}^{-0.75} \cdot P_{CO_2,cat}^{0.5} + C_2 \cdot e^{\frac{\Delta H_{C2}}{RT}} \cdot C_{CO_2,cat}^{-1} \tag{21}$$

$$R_{ir} = C_{ir} \cdot e^{\frac{\Delta H_{ir}}{RT}} \tag{22}$$

where R is the resistance ($\Omega\ m^{-2}$), C_i is the parameter related to electrodes and electrolytes, P_i and ΔH are the pressure (atm) and the enthalpy (J mol^{-1}) respectively.

The electrical power generated by the stack $\dot{W}_{MCFC}$(kW) is expressed as follows:

$$\dot{W}_{MCFC} = V_{cell} \cdot j \cdot A \tag{23}$$

The thermal energy generated within the MCFC stack by electrochemical and water gas shift reactions can be achieved from:

$$\dot{Q}_{gen,MCFC} = I\Delta V_{loss} + T\Delta S \tag{24}$$

where

$$\Delta S = y\left[\left(\bar{s}^0_{H_2O} - \bar{s}^0_{H_2O} - \frac{1}{2}\bar{s}^0_{H_2O}\right) - \overline{R}\ln\ \frac{P_{H_2O}}{P_{H_2}P_{O_2}^{0.5}}\right] \tag{25}$$

where $\bar{s}^0$ is the entropy at standard temperature and pressure.

$$\dot{Q}_{WGS} = x\left(\bar{h}_{CO_2} + \bar{h}_{H_2} - \bar{h}_{CO} - \bar{h}_{H_2O}\right) \tag{26}$$

The net thermal energy of MCFC used to heat up the MCFC anodic and cathodic outlets can be determined as follows:

$$\dot{Q} = \dot{Q}_{gen,MCFC} - \dot{Q}_{WGS} \tag{27}$$

However, it is possible to calculate this quantity from another way. Considering the rate of enthalpy changes of reactants and products at the cathodic and anodic sides, the amount of heat is:

$$\dot{Q}' = \dot{m}_{12}h_{12} + \dot{m}_{13}h_{13} - \dot{m}_{14}h_{14} - \dot{m}_{15}h_{15} \tag{28}$$

Writing energy balance equation over the MCFC stack, the temperature of the stack can be determined through an iterative procedure. The iteration will stop when the desired error is reached:

$$\text{error} = \text{abs}\ \left(\frac{\dot{Q}' - \dot{Q}}{\dot{Q}}\right) < 0.03 \tag{29}$$

To verify the MCFC stack behavior, a comparison has been made on the current density voltage curve generated by the present model and the one reported by Ref. [26]. The highest deviation of cell voltage with respect to the one obtained from reference model is about 3%.

2.3. Exergy analysis

Exergy analysis is based on the second law of thermodynamics and allows one to recognize the location and magnitude of the losses in thermal system [27].

Assuming kinetic and potential exergies are negligible, the exergy flow rate can be expressed as the sum of physical and chemical exergetic terms:

$$\dot{E} = \dot{E}_{Ph} + \dot{E}_{Ch} \tag{30}$$

$$\dot{E}_{Ph} = \dot{m}\left[(h - h_0) - T_0(s - s_0)\right] \tag{31}$$

$$\dot{E}_{Ch} = \dot{n}\left[\sum_k x_k \bar{e}_k^{Ch} + \overline{R}T_0 \sum_k x_k \ln x_k\right] \tag{32}$$

The equations for determining the quantity of exergy destruction in each component of the system can be found in previous works dealing with exergetic analysis of fuel cell based systems [13,18].

Table 1
The cost functions of various components in the MCFC-hybrid plant [9,10,24].

System component	Capital cost function
Compressor	$Z_C = \frac{39.5 \times \dot{m}_a}{0.9 - \eta_c}\left(\frac{p_{dc}}{p_{suc}}\right)\ln\left(\frac{p_{dc}}{p_{suc}}\right)$
Combustion chamber	$Z_{CC} = \left(\frac{46.08 \times \dot{m}_{in}}{0.995 - \frac{p_{out}}{p_{in}}}\right)[1 + \exp(0.018T_{out} - 26.4)]$
Turbine	$Z_T = \dot{W}_T[1318.5 - 98.328\ln(\dot{W}_T)]$
Reformer	$Z_R = 2860A_R^{0.69} + 28940V_R$
Heat exchanger	$Z_{HE} = 130\left(\frac{A_{HE}}{0.093}\right)^{0.78}$
Auxiliary device	$Z_{MCFC,aux} = 0.1(Z_{MCFC})$
MCFC stack	$Z_{MCFC} = 2600 \cdot \dot{W}_{MCFC}$
Burner	$Z_{CC} = \left(\frac{46.08 \times \dot{m}_{in}}{0.995 - \frac{p_{out}}{p_{in}}}\right)[1 + \exp(0.018T_{out} - 26.4)]$

2.4. Economic analysis

The presented economic analysis takes into account both the capital and maintenance costs of components and the operational cost of the plant. The capital cost of each component (Z_k) is estimated based on the cost functions which are listed in Table 1 [9,10,24]. The cost of a component is dependent on design parameters of the component and some operating conditions.

As the MCFC is an emerging technology, current costs are very high. The target cost for MCFC has been estimated to be 2600 €/kW in a previous study [10]. The same value has been considered in the present study. In order to evaluate the capital cost per unit of time ($\dot{Z}_k$):

$$\dot{Z}_k = \frac{Z_k \times \mathrm{CRF} \times \phi}{N \times 3600} \tag{33}$$

where N, ϕ, and CRF are the annual operational hours of the system, maintenance factor, and the Capital Recovery Factor, respectively. CRF can be determined with the following relation:

$$\mathrm{CRF} = \frac{i(1+i)^n}{(1+i)^n - 1} \tag{34}$$

where the terms i and n are the interest rate and system lifetime, respectively. Finally, the operational cost of the whole system can be estimated as follows:

$$\dot{C}_f = \frac{c_f \times \mathrm{LHV} \times \dot{m}_f}{1000} \tag{35}$$

where c_f is the unit cost of the fuel, LHV is the low heating value, and $\dot{m}_f$ is the total mass flow rate of fuel enters the plant.

2.5. Environmental analysis

Nowadays, environmental aspects of power production systems are one of the most important issues which should be taken into account. Environmental legislations are becoming stricter year by year, hence environmental impact of a power generation units should be considered while analyzing these systems. Accordingly, the amounts of CO, NO_x, and CO_2 emissions, based on the calculation procedure explained in Refs. [28–30], are considered as important factors in the present work and their respective social costs are added to the total cost rate of the cycle in the system optimization procedure.

3. System optimization

3.1. Multi-objective optimization

The motivation behind the multi-objective optimization is to look for a set of solutions to problems that are dealing with multiple conflicting objectives simultaneously. Unlike single-objective optimizations, there is no single solution for a multi-objective optimization problem, optimizing each objective simultaneously. Therefore, a set of optimal solutions called Pareto Solution is obtained, which represent trade-offs between the conflicting objectives [31]. In fact, it is the decision-maker's task to find the most preferred Pareto optimal solution according to his/her subjective preferences.

3.2. Genetic algorithms

A genetic algorithm (GA) is a search method employed to find exact or approximate solutions to optimization and search problems based on mechanics of genetics and natural selection inspired by evolutionary theory of Charles Darwin "survival of the fittest" and natural genetics. GA operates with a collection of chromosomes which is called population [32]. Solutions become fitter and fitter as search starts, and finally it converges to a single solution. The most fundamental idea of GA is to imitate the natural evolution process artificially in which populations undergo continuous changes through genetic operators, like crossover, mutation and selection. A comprehensive study on GA can be found in Refs. [33] and [34].

3.3. Objective functions

In the present work, we consider two objective functions. The first one is exergetic efficiency that should be maximized, and the second one is the total cost rate of the whole combined system which should be minimized. Here, the cost of environmental damage is assumed to be added directly to the expenditures that must be paid. Therefore, the second objective function is sum of the economic and environmental objectives. The mathematical formulation of aforementioned objective functions is as follows:

Exergetic efficiency (objective function I)

$$\Psi_{\mathrm{tot}} = \frac{\dot{E}_{\mathrm{out}}}{\dot{E}_{\mathrm{in}}} = \frac{\dot{W}_{\mathrm{MCFC}} + \dot{W}_T - \dot{W}_C + \left(\dot{E}_{22} - \dot{E}_{21}\right)}{\left(\dot{m}_{20} + \dot{m}_5\right) e_f^{\mathrm{CH}}} \tag{36}$$

Total cost rate (objective function II)

$$\dot{C}_{\mathrm{tot}} = \sum_k \dot{Z}_k + \dot{C}_f + \dot{C}_{\mathrm{env}} \tag{37}$$

$$\dot{C}_{\mathrm{env}} = c_{\mathrm{CO}} \dot{m}_{\mathrm{CO}} + c_{\mathrm{CO_2}} \dot{m}_{\mathrm{CO_2}} + c_{\mathrm{NO_x}} \dot{m}_{\mathrm{NO_x}} \tag{38}$$

where $\dot{m}_{\mathrm{CO}}$, $\dot{m}_{\mathrm{NO_x}}$, and $\dot{m}_{\mathrm{CO_2}}$ are the exhaust mass flow rates of carbon monoxide, nitrogen monoxide, and carbon dioxide, and $c_{\mathrm{NO_x}}$, c_{CO} and $c_{\mathrm{CO_2}}$ are the unit damage costs of carbon monoxide, nitrogen monoxide, and carbon dioxide emissions, respectively.

Table 2
List of constraints for system optimization and the range of variation of design parameters.

Constraints	Reason
$2 < r_C < 16$	For typical technology and commercial availability
$0.6 < \eta_C < 0.85$	For typical technology and commercial availability
$0.6 < \eta_T < 0.9$	For typical technology and commercial availability
$0.5 < U_f < 0.9$	Minimum and maximum values of fuel utilization factor
$2.5 < S/C < 4.5$	Minimum and maximum values of steam to carbon ratio
TIT<1250 K	Material temperature limit
T_{MCFC}<1020 K	Material temperature limit
$T_1 > T_4$	For occurring heat exchange between hot and cold streams in HE-1
$T_1 > T_2$	For occurring heat exchange between hot and cold streams in HE-1
$T_2 > T_3$	For occurring heat exchange between hot and cold streams in HE-1
$T_{11} > T_{10}$	For occurring heat exchange between hot and cold streams in RHE
$T_{12} > T_6$	For occurring heat exchange between hot and cold streams in RHE
$T_{23} > 363$ K	To avoid formation of carbonic acid (H_2CO_3) in exhaust gases

3.4. Design parameters and constraints

Optimization of the MCFC hybrid system has been carried out considering the following design variables: turbine inlet temperature (TIT), air compressor pressure ratio (r_C), air compressor isentropic efficiency (η_C), gas turbine isentropic efficiency (η_T), fuel utilization factor (U_f), and steam to carbon ratio (S/C). Table 2 represents design parameters with their ranges as well as other system constraints.

4. Case study

The proposed MCFC-GT hybrid plant as well as the optimization procedure is applied in Tehran, Iran. The ambient pressure and temperature considering in the optimization procedure are 1 bar and 25 °C respectively. The pressure losses within the fuel cell, heat recovery exchanger and recovery heat exchanger are considered to be 4% of the inlet pressure and in the case of combustion chamber the pressure loss is equal to 5% of the inlet pressure. The total power output of hybrid system (combination of MCFC and gas turbine electrical outputs) is estimated to be about 100 kW. The outlet stream (stream 2) contains high amount of thermal energy so its energy is recovered by utilizing the heat recovery exchanger to provide hot water (with temperature of 60 °C) for domestic applications.

In order to determine the CRF (Eq. (34)), the annual interest rate (i), approximate lifetime of the system (n), and the maintenance factor (F) are considered as 14%, 8 years (in case of MCFC stack we consider two 4 years periods by changing the stack after 4 years due to considerable voltage drop), and 1.06, respectively. The annual operational hours of the hybrid system (N) is 8640 h. The unit cost of fuel (c_f) is considered to be 0.004 USD MJ^{-1}. In addition, due to environmental concerns for pollutant emissions 0.02086 USD kg^{-1} CO, 6.853 USD $kg^{-1}NO_x$, and 0.0224 USD $kg^{-1}CO_2$ as penalty are used for carbon monoxide (c_{CO}), nitrogen monoxide (c_{NOx}), and carbon dioxide (c_{CO2}), respectively [24].

5. Results and discussion

5.1. Optimization results

The optimization parameters considered in this study are listed in Table 2. The GA optimization is applied for 120 generations, using a search population size of 300 individuals, cross over probability of 0.9 and gene mutation probability of 0.05. Fig. 2 shows the Pareto frontier solution for the MCFC-GT hybrid plant with the objective functions in the multi objective optimization. The figure evidently displays the competing relation between the two objective functions that led to the obtained Pareto front curve. In this figure, while the total exergetic efficiency of the system increases to about 47%, the total cost rate increases only slightly. Going further and increasing the total exergetic efficiency from 47% to 49% is corresponding to the moderate increase in the cost rate of the plant. More rise in the exergetic efficiency from 49% to the higher values leads to drastic increment in the total cost rate. As it can be observed in Fig. 2, the Pareto front curve represents two ultimate points (points A and B) where the optimization can be considered as a single objective function optimization. The maximum exergetic efficiency exists at design point (A) (54.5%), while the total cost rate is the highest at this point (0.01066 USD s^{-1}). In contrast, the lowest exergetic efficiency is at design point B (44.4%), while the total cost rate has its minimum value at this point (0.01029 USD s^{-1}). Point A represents the situation where the thermodynamic objective (exergetic efficiency) is most weighted, while point B has been mostly weighted in favor of economic objective (total cost rate of the system). It is worth mentioning that in multi-objective optimization and the Pareto solution, each point can be considered as an optimized point. Therefore, selection of the optimum solution depends on preferences and criteria of each decision-maker. In the present work, TOPSIS (Technique for Order Preference by Similarity to an Ideal Solution) decision-making method was utilized to select the final optimum design point [35].

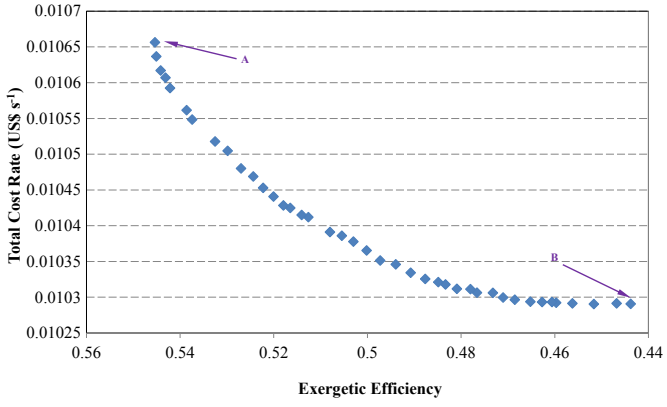

Fig. 2. Pareto optimal frontier from multi-objective optimization of MCFC-GT hybrid plant.

The exergetic efficiency and total cost rate at the final optimum design point, selected by TOPSIS, are 51.7% and 0.01042 USD s^{-1} respectively. The numerical values of optimum design parameters for single-objective and multi-objective optimization methods are listed in Table 4.

Fig. 3 summarizes the exergy destruction rate in different components of the hybrid system at optimum points obtained from three methods of optimization (single-objective function I (exergetic efficiency), single objective function II (total cost rate), and multi-objective functions (both exergetic efficiency and total cost rate)). As it shown in this figure, the highest amount of exergy destruction rate occurs in reformer and burner.

In order to demonstrate the share of the cost of each component in the total capital cost of the plant, Table 3 illustrates the capital cost of each component at optimum points with single-objective I, II, and multi-objective optimization methods. As expected, the most dominant component cost is the MCFC stack cost, and the second highest capital cost is the one contributing to the gas turbine. It is noteworthy to mention that the capital costs of the turbomachinery are much higher than those of heat exchangers, mixers, and combustion chamber. In all three cases (single-objective I, II, and multi-objective optimization) capital cost of MCFC stack is accounted for more than 80% of the total cost.

The performance results of the MCFC-GT plant at 3 optimal design points are presented in Table 4. As expected, the total cost rate associated with the optimal point selected by TOPSIS method is in between those corresponding to only one objective function. The total cost of the hybrid system obtained from objective function I (maximum exergetic efficiency) and objective function II (minimum cost rate) have the highest (0.01066 USD s^{-1}) and lowest (0.01029 USD s^{-1}) values respectively. Furthermore, the optimum values of the system exergetic efficiency with optimizing the single-objective function I, single-objective function II, as well as optimizing multi-objective functions I and II are 51.7%, 44.4%, and 54.5%, respectively. The results show that when only exergetic efficiency is considered as the objective function, the system is optimized only thermodynamically regardless of the total cost rate. Conversely, by considering only the economic aspect of the plant, the cost rate decreases noticeably but

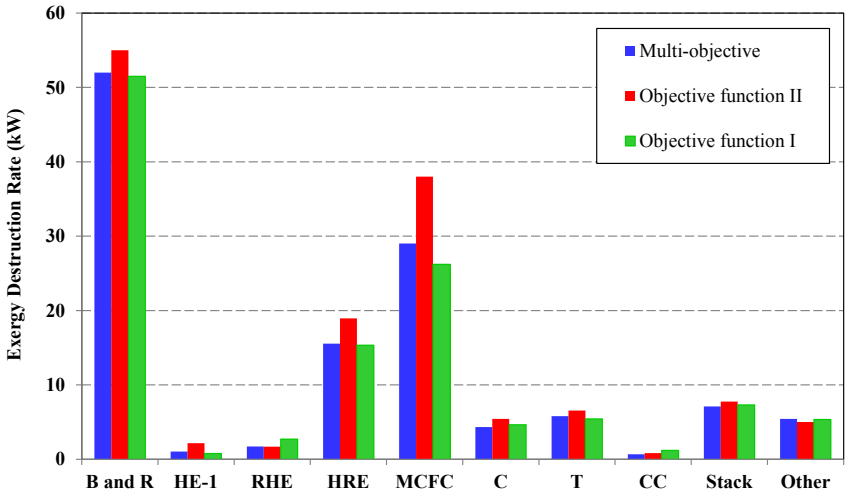

Fig. 3. Exergy destruction rate in various components of the hybrid system.

thermodynamic efficiency of the system will be affected adversely. The multi objective optimization, on the other hand, results in a trade-off between thermodynamic efficiency and total cost rate at the same time.

Furthermore, a sensitivity analysis has been carried out on the impact of fuel unit cost and interest rate on the Pareto front in order to provide a better understanding of the optimization problem. Fig. 4 represents the variation of Pareto front for different values of fuel unit cost. As can be observed from the figure, with increasing the fuel unit cost Pareto front shifts upward and leftward (higher exergetic efficiency) toward higher exergetic efficiencies and cost rates. The upward movement of the Pareto front optimum solutions is due to the fact that increasing the fuel cost results in higher total cost rates. Moreover, it should be noted that at the higher exergetic efficiencies regions (with lower weight of thermodynamic objective) the Pareto front variation is much less sensitive to the fuel cost fluctuations compared to regions with lower exergetic efficiency. Similar behavior can be seen in Fig. 5 which depicts the sensitivity of Pareto front to annual interest rate. As it is vividly shown in the figure, at high exergetic efficiency region, the Pareto fronts at different interest rates almost overlap which indicates the weak dependence of objective functions on costing parameter (i.e. interest rate).

In order to investigate the influence of environmental aspect on the optimum solutions, the same optimization procedure has been performed without including the environmental costs in the total cost rate (second objective function). The final optimum point chosen based on the Pareto solutions obtained by the new definition of the second objective function results in a total cost rate of 0.0096 USD s^{-1} and exergetic efficiency of 48.5%. In fact, the reduction in the total cost and exergetic efficiency is attributed to the fact that, as the environmental cost is not taken into account, less weight is given to the operating cost of the system. This fact moves the selected design to a less efficient optimal design point with lower capital cost and less exergetic efficiency.

Table 3
Capital costs of system major components (in terms of USD).

Component	Point A as an extreme in favor of exergetic efficiency	Point B as an extreme in favor of total cost rate	Multi objective optimization (trade-off approach)
Compressor	6156	3742	7284
Turbine	76036	67445	73293
Reformer	14913	12704	13999
MCFC	536120	412880	486200
Auxiliary	26806	20644	24310
Heat exchangers	6009	5082	5501

5.2. Sensitivity analysis

5.2.1. Steam to carbon ratio (S/C)

As the first analysis, the impact of steam to carbon ratio (S/C) on the exergetic efficiency is investigated and plotted in Fig. 6. This figure reveals a weak influence of the steam to carbon ratio on the exergetic efficiency, with exergetic efficiency mainly improves with increasing steam to carbon ratio. By employing higher S/C ratios, the amount of water for the reforming and water gas shift reactions (reactions (1) and (3) respectively) increases, resulting in the equilibrium shift to the right side due to the Le Chatelier's principle. On one hand, the improvement in the reactions brings about higher hydrogen concentration at the reformer outlet which accordingly improves the electrical efficiency of the fuel cell stack. On the other

Table 4
The optimum values of system design parameters and the corresponding hybrid system performance-related results from three optimization standpoints.

Parameter	Point A as an extreme in favor of exergetic efficiency	Point B as an extreme in favor of total cost rate	Multi objective optimization (trade-off approach)
TIT(K)	1035	1032	1037
MCFC temperature (K)	948	981	963
r_C	6.11	5.42	5.81
$\square_T$	0.9	0.83	0.89
$\square_C$	0.84	0.79	0.85
U_f	0.8	0.63	0.72
S/C	3.09	2.5	3.17
Social cost of air pollution ($ $year^{-1}$)	8075	9702	8489
Electrical power output from turbine (kW)	86.4	75.5	82.9
Electrical power output from MCFC (kW)	103.1	79.4	93.5
Air compressor and pump electrical power (kW)	48.4	47.1	46.0
HRE net exergy gain (kW)	3.6	4.9	2.8
Exergetic efficiency (%)	54.5	44.4	51.7
Total annual cost ($)	331568	320060	324104

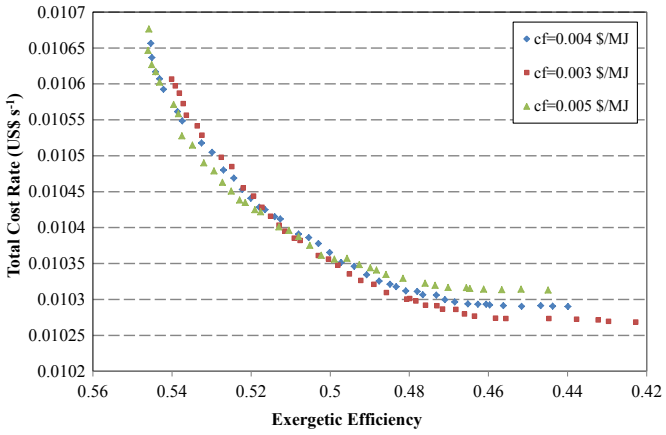

Fig. 4. The sensitivity of Pareto front shape to fuel unit cost.

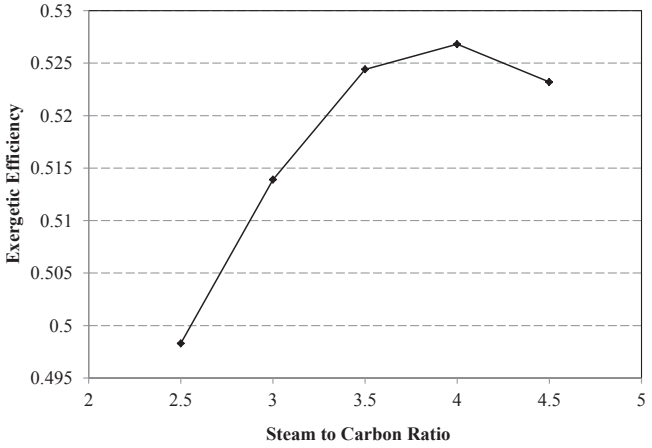

Fig. 6. Effect of S/C variations on exergetic efficiency.

hand, due to the reactants dilution at the reformer outlet, lower temperatures for cogenerative purposes would be expected which reduce the cogeneration efficiency of the plant.

On the other hand, the reactants dilution at the reformer outlet results in a lower corresponding outlet temperature which in turn, in order to keep the TIT constant, requires higher flow rate of auxiliary fuel in the combustion chamber. The mentioned increment in the auxiliary fuel results in higher exergy destructions within the combustion chamber and consequently lower exergetic efficiency of the overall plant. As a result of these contradictory influences of increasing S/C ratio, the graph of exergetic efficiency versus S/C ratio indicates an optimum in S/C = 4.

5.2.2. Compressor pressure ratio (r_C)

Fig. 7 illustrates the effect of the compressor pressure ratio on the exergetic efficiency of the plant. The upward trend of the exergetic efficiency with pressure ratio can be easily observed from the figure. Increasing the operating pressure influences the plant through different ways. Firstly, the reforming reactions tend toward the reactants side, due to the Le Chatelier's principle, which exacerbate the hydrogen production performance within the reformer. On the other hand, at elevated pressures the power and the exergetic efficiency of the MCFC enhance since, according to Eq. (20) and Eq. (21), the increment in the partial pressures of gases and corresponding improvement in the mass transport characteristics of the cell leads to lower cathodic and anodic losses [36] and subsequently higher performance of the cell.

5.2.3. Turbine inlet temperature (TIT)

Fig. 8 shows the variation of overall exergetic efficiency of the system with the turbine inlet temperature (TIT). It can be seen that the overall hybrid system efficiency has a steady decrease with increase in TIT. This behavior is due to the fact that higher TIT requires higher amount of heat provided by the combustion chamber which results in higher exergy destructions within this component. In addition, higher TIT diminishes the total exergetic efficiency since the heat input to the combustor is utilized in a less effective manner than that of the fuel cell [9,37]. It should be pointed out that the major purpose of heating the MCFC outlet stream in the combustion chamber, though it is not beneficial from exergetic point of view, is to obtain a certain power output from the whole cycle.

5.2.4. Current density (j)

The falling trend of exergetic efficiency with increasing current density is depicted in Fig. 9. An increase in the current density incurs lower operating voltage due to the electric losses which also can be concluded from Eq. (14). As a result, higher current densities lead to higher rate of exergy destruction of fuel cell which

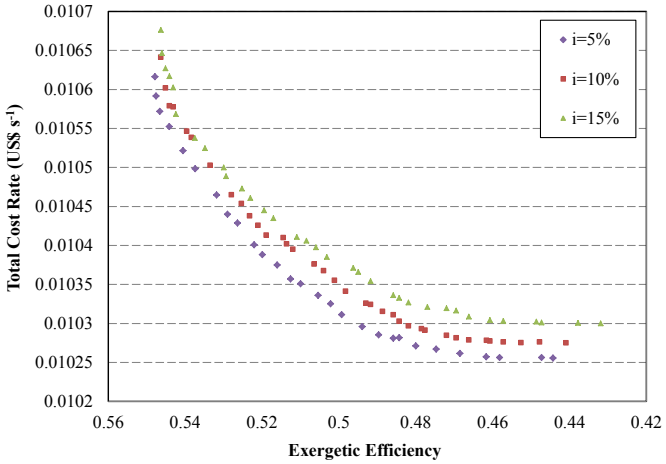

Fig. 5. The sensitivity of Pareto front shape to interest rate.

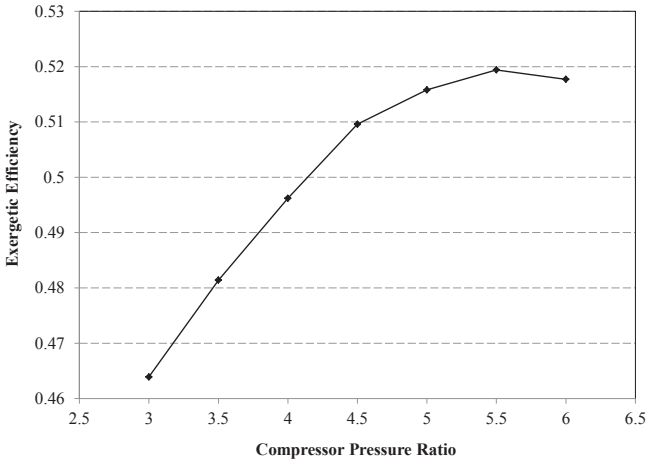

Fig. 7. Effect of compressor pressure ratio variations on exergetic efficiency.

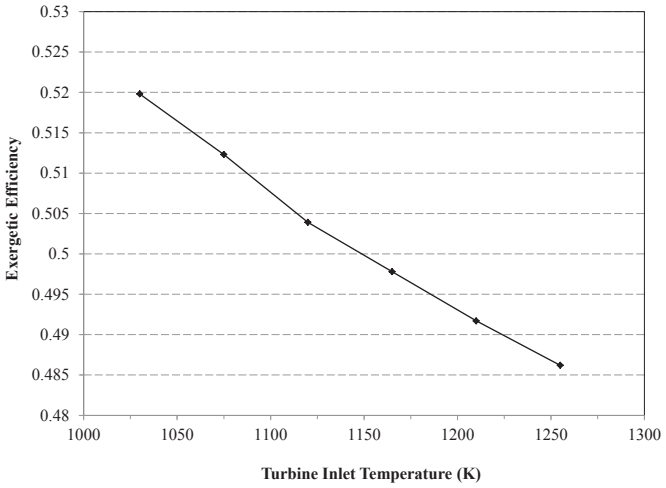

Fig. 8. Effect of turbine inlet temperature variations on exergetic efficiency.

comprises the largest contribution to the total exergy destruction of the plant and subsequently deteriorate the exergy efficiency of the entire plant.

6. Conclusions

The current research encompasses a comprehensive study of an external reforming molten carbonate fuel cell/gas turbine hybrid cycle from exergy, economic, and environmental aspects. The system was modeled and analyzed in MATLAB® environment. Multi-objective optimization of the system was performed using genetic algorithm technique, while considering the total cost rate and the exergetic efficiency of the plant as objective functions. It is noteworthy that for our case study, the exergetic efficiency at the final optimal design point obtained from multi-objective optimization was 51.7%, corresponding to the total cost of 0.324 million USD per year. A sensitivity analysis of the Pareto optimal solutions with change in fuel unit cost and interest rate was also carried out and discussed in detail. Moreover, the sensitivity analysis on variations of key system parameters revealed that the operating pressure has the most significant effect on the exergetic efficiency of the plant.

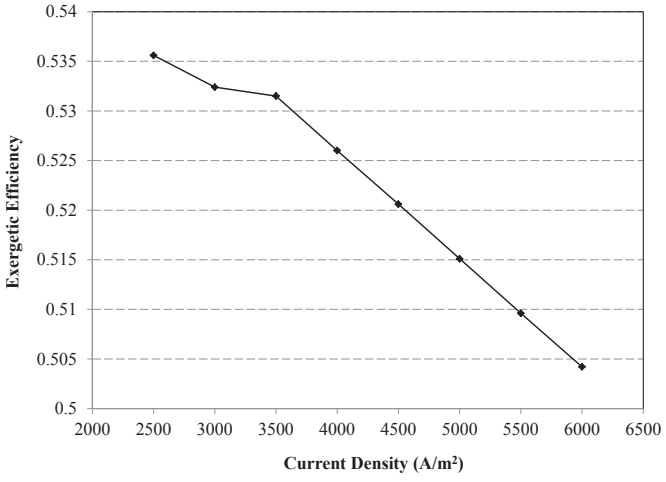

Fig. 9. Effect of current density variations on exergetic efficiency.

References

[1] G. De Simon, F. Parodi, M. Fermeglia, R. Taccani, Simulation of process for electrical energy production based on molten carbonate fuel cells, J. Power Sources 115 (2003) 210–218.

[2] J.W. Pratt, L.E. Klebanoff, K. Munoz-Ramos, A.A. Akhil, D.B. Curgus, B.L. Schenkman, Proton exchange membrane fuel cells for electrical power generation on-board commercial airplanes, Appl. Energy 101 (2013) 776–796.

[3] D.W. Hengeveld, S.T. Revankar, Economic analysis of a combined heat and power molten carbonate fuel cell system, J. Power Sources 165 (2007) 300–306.

[4] M. Miansari, K. Sedighi, M. Amidpour, E. Alizadeh, M. Miansari, Experimental and thermodynamic approach on proton exchange membrane fuel cell performance, J. Power Sources 190 (2009) 356–361.

[5] S. Mekhilef, R. Saidur, A. Safari, Comparative study of different fuel cell technologies, Renew. Sustain. Energy Rev. 16 (2012) 981–989.

[6] J. Brouwer, F. Jabbari, E.M. Leal, T. Orr, Analysis of a molten carbonate fuel cell: numerical modeling and experimental validation, J. Power Sources 158 (2006) 213–224.

[7] R. Rashidi, P. Berg, I. Dincer, Performance investigation of a combined MCFC system, Int. J. Hydrogen Energy 34 (2009) 4395–4405.

[8] P. Heidebrecht, K. Sundmacher, Molten carbonate fuel cell (MCFC) with internal reforming: model-based analysis of cell dynamics, Chem. Eng. Sci. 58 (2003) 1029–1036.

[9] V. Verda, F. Nicolin, Thermodynamic and economic optimization of a MCFC-based hybrid system for the combined production of electricity and hydrogen, Int. J. Hydrogen Energy 35 (2010) 794–806.

[10] A. Sciacovelli, V. Verda, Sensitivity analysis applied to the multi-objective optimization of a MCFC hybrid plant, Energy Convers. Manag. 60 (2012) 180–187.

[11] L. Leto, C. Dispenza, A. Moreno, A. Calabrò, Simulation model of a molten carbonate fuel cell–microturbine hybrid system, Appl. Therm. Eng. 31 (2011) 1263–1271.

[12] X. Zhang, J. Guo, J. Chen, Influence of multiple irreversible losses on the performance of a molten carbonate fuel cell-gas turbine hybrid system, Int. J. Hydrogen Energy 37 (2012) 8664–8671.

[13] R. Rashidi, I. Dincer, P. Berg, Energy and exergy analyses of a hybrid molten carbonate fuel cell system, J. Power Sources 185 (2008) 1107–1114.

[14] A. Liu, Y. Weng, Performance analysis of a pressurized molten carbonate fuel cell/micro-gas turbine hybrid system, J. Power Sources 195 (2010) 204–213.

[15] F. Jurado, Study of molten carbonate fuel cell—microturbine hybrid power cycles, J. Power Sources 111 (2002) 121–129.

[16] S.-Y. Lee, D.-H. Kim, H.-C. Lim, G.-Y. Chung, Mathematical modeling of a molten carbonate fuel cell (MCFC) stack, Int. J. Hydrogen Energy 35 (2010) 13096–13103.

[17] J.M. Muñoz de Escalona, D. Sánchez, R. Chacartegui, T. Sánchez, A step-by-step methodology to construct a model of performance of molten carbonate fuel cells with internal reforming,, Int. J. Hydrogen Energy 36 (2011) 15739–15751.

[18] R.S. El-Emam, I. Dincer, Energy and exergy analyses of a combined molten carbonate fuel cell – Gas turbine system, Int. J. Hydrogen Energy 36 (2011) 8927–8935.

[19] R. Chacartegui, M.J. Blanco, J.M. Muñoz de Escalona, D. Sánchez, T. Sánchez, Performance assessment of molten carbonate fuel cell–humid air turbine hybrid systems, Appl. Energy 102 (2013) 687–699.

[20] P.S. Varbanov, J. Klemeš, R.K. Shah, H. Shihn, Power cycle integration and efficiency increase of molten carbonate fuel cell systems, J. Fuel Cell Sci. Technol. 3 (2006) 375–383.

[21] A.V. Akkaya, B. Sahin, A study on performance of solid oxide fuel cell-organic Rankine cycle combined system, Int. J. Energy Res. 33 (2009) 553–564.

[22] A. Monaco, U. Di Matteo, Life cycle analysis and cost of a molten carbonate fuel cell prototype, Int. J. Hydrogen Energy 36 (2011) 8103–8111.

[23] A. Dicks, A. Siddle, Assessment of commercial prospects of molten carbonate fuel cells, J. Power Sources 86 (2000) 316–323.

[24] A. Shirazi, M. Aminyavari, B. Najafi, F. Rinaldi, M. Razaghi, Thermal–economic–environmental analysis and multi-objective optimization of an internal-reforming solid oxide fuel cell–gas turbine hybrid system, Int. J. Hydrogen Energy 37 (2012) 19111–19124.

[25] J. Xu, G.F. Froment, Methane steam reforming, methanation and water-gas shift: I. Intrinsic kinetics, AIChE J. 35 (1989) 88–96.

[26] M. Baranak, H. Atakül, A basic model for analysis of molten carbonate fuel cell behavior, J. Power Sources 172 (2007) 831–839.

[27] T.J. Kotas, The Exergy Method of Thermal Plant Analysis, Krieger Publication Co., Florida, 1995.

[28] O.L. Gulder, Flame temperature estimation of conventional and future jet fuels, J. Eng. Gas. Turb. Power 108 (1986) 376–380.

[29] B. Najafi, H. Najafi, M.D. Idalik, Computational fluid dynamics investigation and multi-objective optimization of an engine air-cooling system using ge-netic algorithmProceedings of the Institution of Mechanical Engineers, Part C – J. Mech. Eng. Sci. 225 (2011) 1389–1398.

[30] N.K. Rizk, H.C. Mongia, Semi analytical correlations for NOx, CO and UHC emissions, J. Eng. Gas. Turb. Power 115 (1993) 612–629.

[31] T. Selleri, B. Najafi, F. Rinaldi, G. Colombo, Mathematical modeling and multi-objective optimization of a mini-channel heat exchanger via genetic algorithm, J. Therm. Sci. Eng. Appl. 5 (2013) 031013.
[32] H. Najafi, B. Najafi, P. Hoseinpoori, Energy and cost optimization of a plate and fin heat exchanger using genetic algorithm, Appl. Therm. Eng. 31 (2011) 1839–1847.
[33] D. Goldberg, Genetic Algorithms in Search, Optimization, and Machine Learning, Addison-Wesley Professional, 1989.
[34] J.H. Holland, Adaptation in Natural and Artificial Systems, University of Michigan Press, 1975.
[35] H. Sayyaadi, R. Mehrabipour, Efficiency enhancement of a gas turbine cycle using an optimized tubular recuperative heat exchanger, Energy 38 (2012) 362–375.
[36] G. Simader, Fuel Cells and Their Applications, John Wiley & Sons, Incorporated, 2005.
[37] H. Uechi, S. Kimijima, N. Kasagi, Cycle analysis of gas turbine–fuel cell cycle hybrid micro generation system, J. Eng. Gas Turbines Power 126 (2004) 755–762.